Author(s): Berseneva, Natalia & Gulans, Andris & Krasheninnikov, Arkady V. & Nieminen, Risto M.

Title: Electronic structure of boron nitride sheets doped with carbon from first-principles calculations

Year: 2013

Version: Final published version

Please cite the original version:

Berseneva, Natalia & Gulans, Andris & Krasheninnikov, Arkady V. & Nieminen, Risto M. 2013. Electronic structure of boron nitride sheets doped with carbon from first-principles calculations. Physical Review B. Volume 87, Issue 3. 035404/1-9. ISSN 1550-235X (electronic). DOI: 10.1103/physrevb.87.035404.

Electronic structure of boron nitride sheets doped with carbon from first-principles calculations

Natalia Berseneva,[1] Andris Gulans,[1] Arkady V. Krasheninnikov,[1,2] and Risto M. Nieminen[1]
[1]*COMP Centre of Excellence and Department of Applied Physics, P.O. Box 11100, FI-00076 Aalto University, Espoo, Finland*
[2]*Department of Physics, University of Helsinki, P.O. Box 43, FI-00014, Finland*
(Received 15 May 2012; published 2 January 2013)

Using density functional theory with local and non-local exchange and correlation (XC) functionals, as well as the Green's function quasiparticle (GW) approach, we study the electronic structure of hexagonal boron nitride (*h*-BN) sheets, both pristine and doped with carbon. We show that the fundamental band gap in two-dimensional *h*-BN is different from the gap in the bulk material, and that in the GW calculations the gap depends on the interlayer distance (separation between the images of the BN layers within the periodic supercell approach) due to the non-local nature of the GW approximation, so that the results must be extrapolated to infinitely large separations between the images. We further demonstrate by the example of carbon substitutional impurities that the local and hybrid XC functionals give a qualitatively correct picture of the impurity states in the gap. Finally, we address the effects of many important parameters, such as the choice of chemical potential, and atom displacement cross sections for the substitutional process during electron-beam-mediated doping of *h*-BN sheets with carbon atoms. Our results shed light on the electronic structure of pristine and doped *h*-BN and should further help to optimize the postsynthesis doping of boron nitride nanostructures stimulated by electron irradiation.

DOI: 10.1103/PhysRevB.87.035404 PACS number(s): 81.05.ue, 73.20.Hb, 73.22.−f, 61.72.−y

I. INTRODUCTION

Isolation of single sheets of graphene,[1] a truly two-dimensional (2D) material, and the discovery of its unique properties[2] have given rise to vigorous research of other 2D systems.[3–5] Among them, a structural analog of graphene, a single sheet of hexagonal boron nitride (*h*-BN) comprised of alternating boron and nitrogen atoms, has received particular attention.[6–9] Similar to graphene, *h*-BN has excellent mechanical properties and high thermal conductivity, while its electronic structure is different: in comparison to semimetallic graphene with zero band gap, 2D *h*-BN is a wide (more than 5 eV) band gap semiconductor (see Ref. 10 for an overview of the properties of BN nanostructures).

Both graphene[11–14] and 2D *h*-BN[15,16] can be grown using the chemical vapor deposition (CVD) technique. Keeping in mind the similarities between the atomic structures of these systems (the mismatch between the lattice constants of the materials is only 2%) and the radically different electronic properties, the growth of doped BN and hybrid boron carbon nitride (BCN) materials with tunable electronic characteristics has been attempted.[17] However, although the growth of N-doped graphene has been successfully demonstrated,[18,19] the hybrid BCN material has proven to be thermodynamically unstable with regard to segregation to graphene and *h*-BN,[20–22] so that the growth of homogeneous structures has not been achieved. At the same time, CVD does not provide enough spatial control over the growth of the structures, making impossible the development of well-defined graphene and BN regions within a single sheet, the composite structures which have been predicted[23–27] to have peculiar electronic and magnetic properties.

A different approach to the development of hybrid BCN materials was recently demonstrated.[28,29] The method was based on the postsynthesis substitutional carbon doping of *h*-BN sheets[29] and BN nanotubes[28] via *in situ* electron-beam irradiation inside a transmission electron microscope (TEM). It was found that carbon atoms coming from the decomposition of hydrocarbon molecules (intentionally added to the TEM chamber) under the 300 keV electron beam take the positions of boron atoms; see Fig. 1(a). Using essentially the same technique, C impurities were also introduced into BN sheets at electron energies of 60 keV.[30]

It was later theoretically shown[31] that the main driving force for the substitution is the energetics of the system, as it costs less energy to substitute a B atom than an N atom, especially when the system is becoming charged due to the electron-beam irradiation. The kinetic effects (the displacement rates for B and N atoms) could not fully explain the preferential substitution of B atoms, as at an acceleration voltage of 300 kV the rates are roughly the same for B and N atoms.[32] Considering the possibility of creating triangular holes[9] in the *h*-BN sheet, shown in Fig. 1(b), it was also suggested that a focused electron beam could be employed to create triangular carbon islands or straight ribbons embedded into the BN matrix, as schematically shown in Fig. 1(c), either through beam-mediated substitution reactions or by "filling up" the holes. The theoretical analysis[31] of the substitution process was based on first-principles calculations of formation energies of various substitutional carbon impurities in the *h*-BN matrix. The formation energies of defects in finite supercells were computed for different charge states as functions of electron chemical potentials within the framework of density functional theory (DFT), using local and hybrid exchange and correlation (XC) functionals. The simulation setup and its adequacy for describing the experimental conditions were discussed later on,[33,34] eventually giving rise to a question of how well the DFT approach describes the electronic structure of *h*-BN with carbon impurities.

The main goal of this paper is to study the electronic structure of an *h*-BN sheet with carbon substitutional impurities using advanced techniques such as DFT with hybrid functionals and Green's function quasiparticle (GW) methods. We first carefully simulate the electronic structure of the pristine 2D *h*-BN material and study the convergence of the

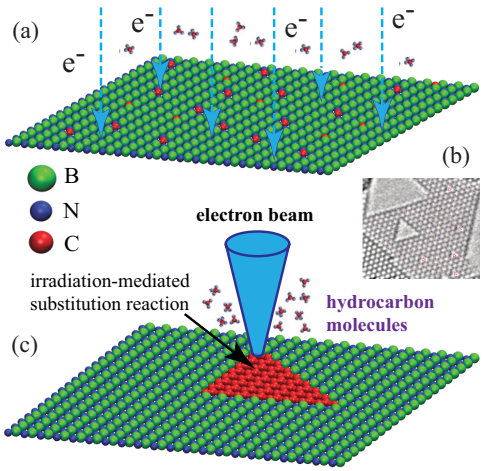

FIG. 1. (Color online) Schematic representation of the electron-beam-mediated substitutional doping of boron nitride monolayer. Hydrocarbon molecules decomposed by the beam provide carbon atoms, which preferentially substitute boron atoms displaced by the beam or due to a beam-induced substitution reaction. (a) Irradiation of the whole sample as experimentally done in Ref. 29. (b) Experimental TEM image of triangular holes formed in a single BN sheet due to the electron beam, provided by Meyer *et al.*[9] (c) Possible way of engineering carbon islands in the BN matrix with a focused electron beam.

results with regard to the most important parameters. We show that due to the non-local nature of the GW approximation, the calculated fundamental band gap in 2D *h*-BN depends on the interlayer distance in the simulation supercell (that is the separation between the images of the *h*-BN sheet within the periodic supercell approach), and that the results must be extrapolated to infinitely large separation between the images. We also show, that contrary to what has been assumed in many papers, the band gaps of bulk and 2D *h*-BN systems differ by more than 0.5 eV. We further demonstrate, by the example of single- and four-carbon-atom substitutional impurities, that the local and hybrid XC functionals give a qualitatively correct picture of the impurity states in the gap. Finally, we address the effects of many important parameters such as the choice of chemical potential, interlayer distance, displacement cross section of electron-beam-mediated substitution process, and the charge state of the system.

II. COMPUTATIONAL METHODS

We carried out first-principles spin-polarized plane-wave electronic-structure calculations within density functional theory, as implemented in the VASP[35] code. We used projector-augmented wave potentials to describe the core electrons and the generalized gradient approximation of Perdew-Burke-Ernzerhof (PBE)[36] to account for the exchange-correlation energy of interacting electrons. As the PBE approach normally underestimates the band gap and thus may give rise to incorrect positions of the impurity levels, more accurate results were obtained with the use of the hybrid Heyd-Scuseria-Ernzerhof (HSE) functional.[37] To confirm the results, we carried out even more rigorous G_0W_0, GW_0, and GW (Refs. 38,39) calculations on top of the PBE data. Structural optimizations of all geometries were performed by the conjugate-gradient scheme until the maximum allowed force acting on each atom was less than 0.02 eV/Å. In most of the calculations, the one-electron Kohn-Sham wave functions were expanded over a plane-wave basis with a kinetic energy cutoff of 400 eV. We further studied the dependence of the results on the kinetic energy cutoff, as described in Sec. III A.

In this work, we investigate both neutral and charged states of the *h*-BN system with impurity atoms. Supercells of different sizes (2, 18, 32, and 72) with different numbers of B and N atoms substituted with C atoms were employed. In order to prevent spurious interlayer interaction within the periodic supercell simulation scheme, we used a vacuum spacing between adjacent 2D *h*-BN layers (in the direction normal to the sheet) of 10 Å. The dependence of the results on vacuum spacing was tested, as described in Secs. III A and III B. In the total-energy calculations, **k** points in the Brillouin zone (BZ) were generated by the Monkhorst-Pack scheme with a Γ-centered grid. The optimal number of **k** points used to sample the BZ was determined by a series of convergence tests. Particularly, we used $6 \times 6 \times 1$, $4 \times 4 \times 1$, and $6 \times 6 \times 3$ Γ-centered **k**-point meshes for computing, respectively, the 3×3 (18 atoms), 4×4 (32 atoms)/6×6 (72 atoms), and bulk *h*-BN with AB stacking. Such a simulation setup has been demonstrated to be adequate for the modeling of defects and impurities in 2D systems with covalent bonding.[32,40,41] DFT molecular dynamics (MD) simulations of atom dynamics after electron impacts were carried out as in Refs. 32 and 42.

III. RESULTS AND DISCUSSION

A. Electronic structure and band gap of the pristine *h*-BN sheet

Although the electronic structure of bulk and 2D *h*-BN materials has been studied at length,[39,43–45] both experimentally and theoretically, the reported results differ considerably from each other. Theoretical estimates of the gap for an isolated *h*-BN sheet vary from 4.6 to 7.1 eV,[39,45–48] depending on the simulation method used. Experimental data also vary from 4.6 to 7.0 eV.[49] Moreover, it was assumed in many works that the gap of 2D *h*-BN is the same as in bulk 3D material. Interestingly enough, in spite of a large number of experiments on the electronic properties of bulk *h*-BN (see Refs. 50 and 51 and references therein), neither the direct or indirect band gap is accurately known: the values reported in the literature range from 3.6 to 7.1 eV; see Ref. 51. Putting aside uncertainties in the stacking order of the layers affecting the electronic structure,[46] different experimental techniques (optical/transport measurements) used to measure the gap, and strong excitonic effects in *h*-BN (which should decrease the gap by nearly 1 eV),[44] it is desirable to have the accurate theoretical value for a single *h*-BN sheet obtained from the GW calculations. Although such calculations have already been carried out,[39] the convergence of the results with regard to the most important parameters, such as the amount of vacuum between the images of the sheet (within the periodic supercell approach) and the number of empty states accounted for, has not been studied before.

In order to accurately assess the gap of the isolated *h*-BN sheet and get further insight into the electronic properties

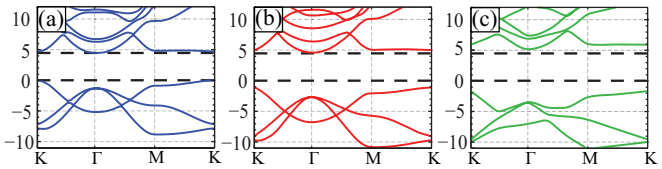

FIG. 2. (Color online) (a) PBE, (b) HSE, and (c) G_0W_0 band structure for pristine h-BN sheet (2-atom unit cell) with 10 Å vacuum layer thickness. The top of the valence band within the PBE is taken as zero energy. The edges of the PBE band gap are indicated by black dashed horizontal lines. The Greek letters stand for high-symmetry points in the BZ of the supercell.

of BN sheets with carbon impurities, as well as to better understand the accuracy of the defect formation energy estimates, we started by calculating the band structures of the pristine material. The band structures of the h-BN sheet were first calculated using the PBE and HSE approaches. The results are presented in Fig. 2. The values of 4.56 and 5.56 eV for the band gap of the h-BN sheet (indirect $K - \Gamma$ gap) were obtained within the PBE and HSE functionals, respectively.

We also calculated the quasiparticle band gap of the h-BN sheet within the framework of the GW approximation using the PBE data as input. We carried out not only the single-shot G_0W_0 simulations [Fig. 2(c)], but also studied the role of self-consistency in the quasiparticle spectra and applied the GW_0 and GW methods.[38,39]

The numerical reliability of existing many-body studies of bulk and single-layer BN[45,52–55] is unclear in light of recent GW calculations done by Friedrich *et al.* and Shih *et al.*[56,57] They considered quasiparticle spectra of ZnO and showed that the calculated band gap is very sensitive to the number of conduction bands included and the expansion of the dielectric function. In order to avoid these pitfalls, we carefully studied the convergence issues in the context of single-layer h-BN.

The GW module of the VASP package uses the plane-wave basis in the description of the dielectric function.[58] This basis is limited by the dielectric function energy cutoff $q^2/2$ (different from the plane-wave cutoff energy), where q is the absolute value of the largest wave vector used in the representation. It can be shown[59] that the quasiparticle energies $\varepsilon^{\mathrm{QP}}$ converge as

$$\varepsilon^{\mathrm{QP}}(q) = \varepsilon^{\mathrm{QP}}(q \to \infty) + \frac{A}{q^3} + \frac{B}{q^5} + O\left(\frac{1}{q^6}\right), \qquad (1)$$

where A and B are numerical constants. A detailed discussion of Eq. (1) will be given elsewhere.[59] In the present paper, we only mention that the slow convergence of quasiparticle energies can be explained by the divergent electron-electron repulsion.

In practical GW calculations, we use different GW cutoff energies. Then, quasiparticle energies are fitted to the form $\varepsilon^{\mathrm{QP}}(q) \approx \varepsilon^{\mathrm{QP}}(q \to \infty) + \frac{A}{q^3} + \frac{B}{q^5}$. This procedure allows us to extrapolate the results to the complete-basis limit. Previous BN studies did not apply any strategies to estimate how the dielectric function representation affects the quasiparticle spectra.

Equation (1) underlines the contribution of rapidly varying states. Clearly, omitting high-energy conduction states at GW calculations leads to an additional error. Its magnitude depends on q: the higher the q, the more empty states are required to reach the desired accuracy. Thus, the q-extrapolation procedure described above must be applied carefully.

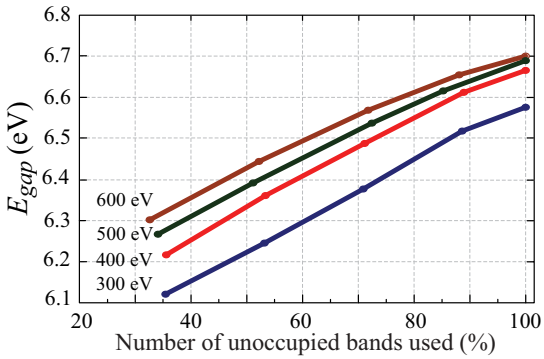

FIG. 3. (Color online) The band gap extrapolated to the complete-basis limit as a function of the number of unoccupied states accounted for at different plane-wave cutoff energies calculated using G_0W_0 for h-BN with 10 Å vacuum layer thickness. The labels stand for different plane-wave cutoff energies used for the representation of the Kohn-Sham eigenstates.

The contribution of discarded high-energy bands is illustrated in Fig. 3. A limited number of unoccupied states results in an underestimated quasiparticle band gap. For instance, using 30% of the conduction states leads to an error of 0.4 eV. Having explored numerical convergence issues, we use all available unoccupied states and perform the extrapolation to the complete basis limit in further G_0W_0, GW_0, and GW calculations.

The obtained G_0W_0, GW_0, and GW quasiparticle gaps for bulk h-BN (AB stacking) are 6.07, 6.41, and 6.90 eV, respectively. The band gap increases with each level of self-consistency, and this observation is in agreement with the trends observed in Refs. 38 and 39.

Apart from purely numerical issues, we also considered how the band gap depends on the thickness of the vacuum layer between the images of the h-BN sheet. As the separation between h-BN layers increases, the PBE/HSE band gap quickly saturates to the monolayer limit, as shown in Fig. 4.

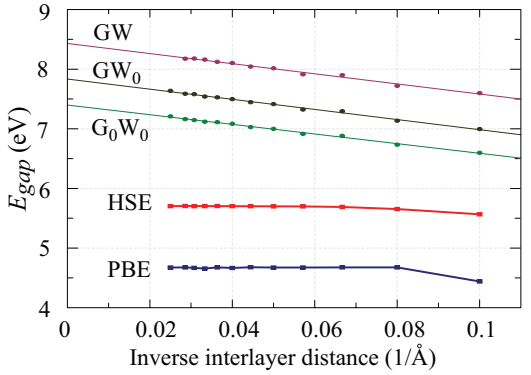

FIG. 4. (Color online) The band gap as a function of the inverse distance between the sheets (vacuum spacing between the images of the sheets). Dots are the results of the PBE, HSE, G_0W_0, GW_0, and GW calculations; the lines stand for extrapolations.

TABLE I. Calculated and experimental results for bulk and planar (2D) BN.

Structure	$E_{g_{G_0W_0}}$ (eV)	$E_{g_{GW_0}}$ (eV)	$E_{g_{GW}}$ (eV)	Expt. value (eV)	Refs.
Bulk	6.07	6.41	6.90	3.6–7.1	50, 51
2D	7.40	7.83	8.43	4.6–7.0	49

The situation is different in the GW calculations. The G_0W_0, GW_0, and GW band gaps for an isolated h-BN sheet (at 10 Å vacuum separation) are 6.60, 7.00, and 7.60 eV, respectively. The G_0W_0 value agrees well with the results reported in Ref. 47. However, it is evident from Fig. 4 that the band gaps calculated at 40 Å of the interlayer separation in h-BN are different from the values calculated at 10 Å and still differ from the limit of infinite separation. This behavior contrasts with the PBE and HSE data, where a separation of 15 Å is sufficient to obtain a converged band gap.

Such a difference between PBE/HSE and all three quasiparticle methods can be explained by non-local screening effects, which are described with the GW formalism, but cannot be captured with PBE and HSE. For a detailed discussion of the physics behind this effect, we refer to Refs. 60 and 61. In the limit of large separations d between h-BN layers, the GW band gap converges as $1/d$, and we use this dependence for extrapolation. Truncation of the Coulomb interaction in the direction perpendicular to the sheets may also be a solution to this problem.

The G_0W_0, GW_0, and GW band gaps for an isolated h-BN sheet (at infinite separation) are 7.40, 7.83, and 8.43 eV, respectively. It is obvious that the band gaps for bulk and monolayer h-BN differ by more than 0.5 eV (see also Table I).

B. Electronic structure and band gap of the h-BN sheet with carbon impurities

Having analyzed the electronic structure of the pristine h-BN sheet, we calculated the band structures of doped BN sheets with triangular-shaped substitutional carbon defects.[31] Examples of investigated configurations are shown in Fig. 5. Throughout this paper, we use the following notations: C_B means that a single B atom was substituted with a C atom, while $4C_{3B1N}$ stands for a triangular island formed by substituting three B and one N atoms with four C atoms, etc.

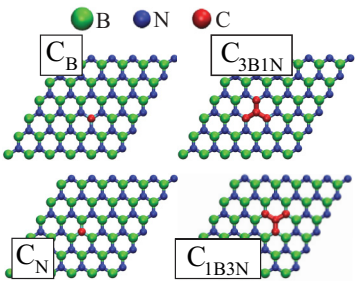

FIG. 5. (Color online) Examples of several structures studied in our work, including single carbon atom substitutional impurities (C_B and C_N) in the h-BN sheet and four carbon atom islands with boron ($4C_{1B3N}$-structure) and nitrogen ($4C_{3B1N}$-structure) termination.

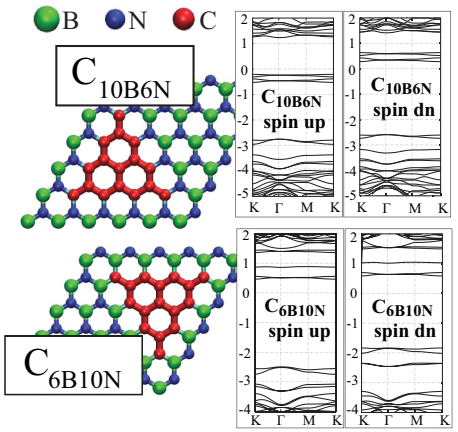

FIG. 6. (Color online) Examples of the structures with larger carbon triangular substitutional impurities in the h-BN sheet with boron ($16C_{6B10N}$) and nitrogen ($16C_{10B6N}$) termination together with calculated PBE-based band structures (spin-up and spin-down results are presented). The Greek letters stand for high-symmetry points in the BZ of the supercell.

In Fig. 7, we present PBE and HSE band structures for 32-atom supercells with substitutional defects composed from one to four carbon atoms (C_B, C_N, $4C_{3B1N}$, $4C_{1B3N}$) inserted into the h-BN host matrix. The PBE and HSE pictures are qualitatively the same, which explains the good agreement between the HSE and PBE formation energies of the defects reported earlier.[31] New states associated with defects appear in the gap, either deep states close to the middle of the gap or shallow states close to the band edges. It is obvious that the larger the defect size, the more new states appear in the band gap (Fig. 6). Defects with the preferential substitution of B atoms (e.g., $4C_{3B1N}$) give rise to occupied states (for zero electron chemical potential), while those with the preferential substitution of N atoms (e.g., $4C_{1B3N}$ structure) give rise to empty states.

We also carried out quasiparticle G_0W_0 calculations for single-atom impurities. The band structures for a 18-atom system (at 10 Å interlayer separation) with C_B and C_N defects are shown in Fig. 8. The positions of the impurity levels qualitatively agree well for PBE, HSE, and G_0W_0 calculations. In addition, we considered the band structure dependence on the thickness of the vacuum layer between the images of the h-BN sheets. Due to the high computational cost, only calculations with 12.5 and 15 Å vacuum layer separation were carried out for an 18-atom system with C_B and C_N defects. We conclude that with increasing the interlayer distance, the impurity level moves up in energy (towards the conduction band edge).

C. Defect formation energies: The role of chemical potential

The substitutional carbon defects can appear in various charge states q. The formation energy E_f of a defect composed of K_C carbon atoms inserted to replace K_B boron and K_N nitrogen atoms ($K_B + K_N = K_C$) in the h-BN

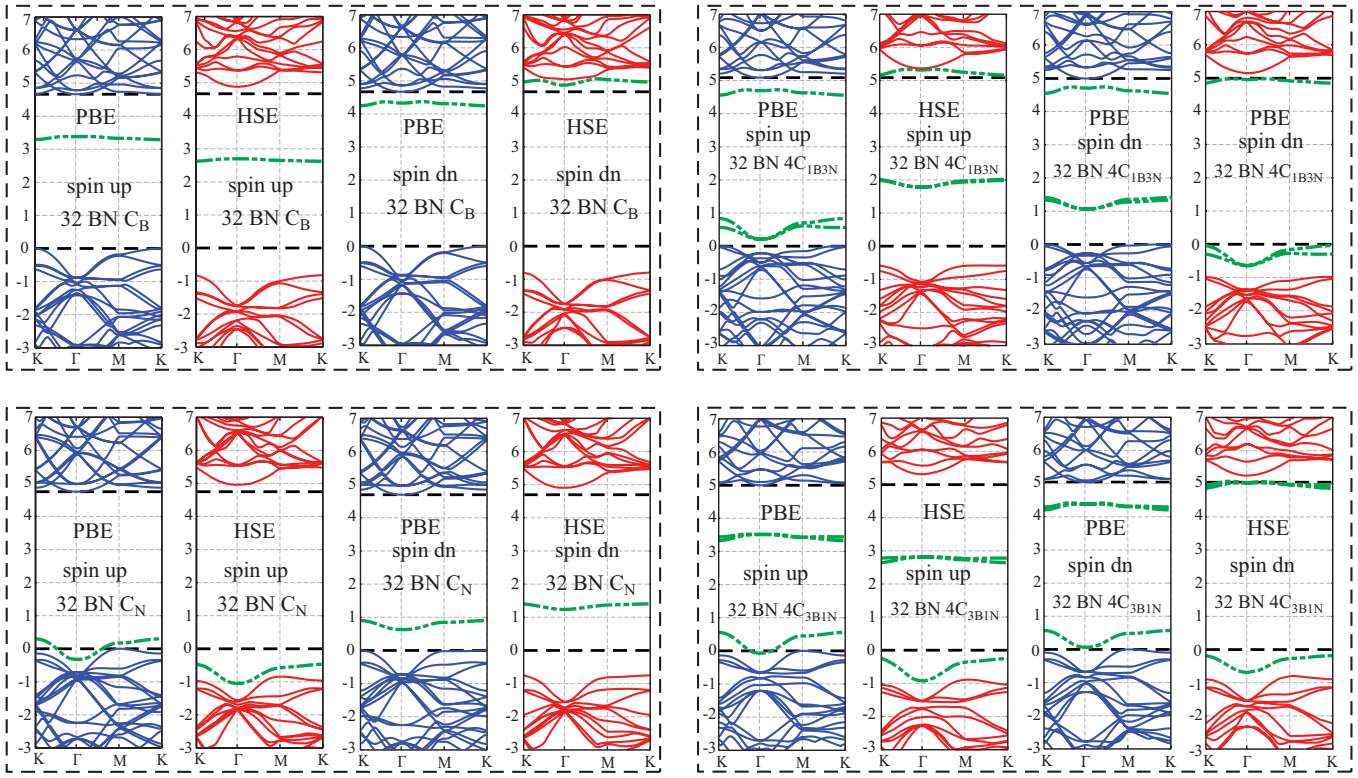

FIG. 7. (Color online) Band structures of 32-atom supercells with substitutional defects composed from one to four carbon atoms (C_B, C_N, $4C_{3B1N}$, $4C_{1B3N}$ defects) inserted into the *h*-BN host matrix. Calculations are done involving PBE (blue lines) and HSE (red lines) approaches. Green dotted lines emphasize the impurity levels. Spin-up and spin-down results are presented. The top of the valence band within the PBE is taken as zero energy. The edges of the PBE band gap are indicated by black dashed horizontal lines. The Greek letters stand for high-symmetry points in the BZ of the supercell.

matrix is

$$E_f\left(K_C^q\right) = E_{\text{tot}}\left(K_C^q\right) - E_{\text{tot}}(\text{BN}) + K_B\mu_B + K_N\mu_N - K_C\mu_C + q(\mu_e - E_V), \quad (2)$$

where $E_{\text{tot}}(K_C^q)$ and $E_{\text{tot}}(\text{BN})$ are the calculated total energies of defected and defect-free BN systems, respectively. q is the charge state of the defect complex, E_V is the energy position of the valence band maximum, and μ_e is the electron chemical potential (defined within the band gap with respect to the E_V). μ_B, μ_N, and μ_C are the chemical potentials of the elements present in the system. In equilibrium,

$$\mu_{\text{BN}} = \mu_B + \mu_N, \quad (3)$$

where μ_{BN} is the total energy per BN pair in a pristine *h*-BN sheet. μ_C is chosen as the energy per atom in a C monolayer (graphene sheet). The choice of μ_B and μ_N is defined by the growth conditions of BN sheets, such as stoichiometry between the components.

A previous work[31] showed that under N-rich conditions, the substitution of B atoms with C atoms costs less than the substitution of N atoms. For the neutral charge states, the difference in energy is about 2 eV in favor of B for single-atom defects. When a single B (N) atom is substituted with a C atom, one extra electron is added (removed) and the dominant charge states of the C_B and C_N defects are +1, 0, and −1. The larger defect islands can support higher charge states. Positive charging further lowers the formation energy of C_B defects, while negative charging favors C_N.

There are many factors that may affect the growth process during material manufacture. Therefore, defining the proper parameters and environmental conditions is crucial. The correct choice of the environmental conditions is also very important for electron-beam-mediated postsynthesis doping. Even though an N-rich environment better matches the described experimental situation, we also investigated how the results depend on the choice of boron chemical potential by the example of single substitutional impurities (C atom in B- and N-atom positions). We varied μ_B up to the value for bulk material (B-rich environment). The calculated E_f of C_B and C_N defects for the neutral charge states are presented in Fig. 9 as functions of μ_B. The horizontal lines are formation energies for a single carbon impurity under N-rich conditions. The lines that indicate the E_f behaviors of C_B and C_N in a B-rich environment intersect (Fig. 9). This crossing point separates the region where the substitution of B (left from the point) is preferable over N substitution. Contrarily, the substitution of N atoms becomes preferable at μ_B growing (right from the point) towards the energy of an isolated B atom. The value of $\mu_B = -7.62$ eV corresponds to the lowest energy α-rhombohedral phase of boron. It is computed as a sum of the energy of an isolated atom in our model and the cohesive energy of the α phase.[62] It should be emphasized that the selected potential of the μ_B is close to the crossing

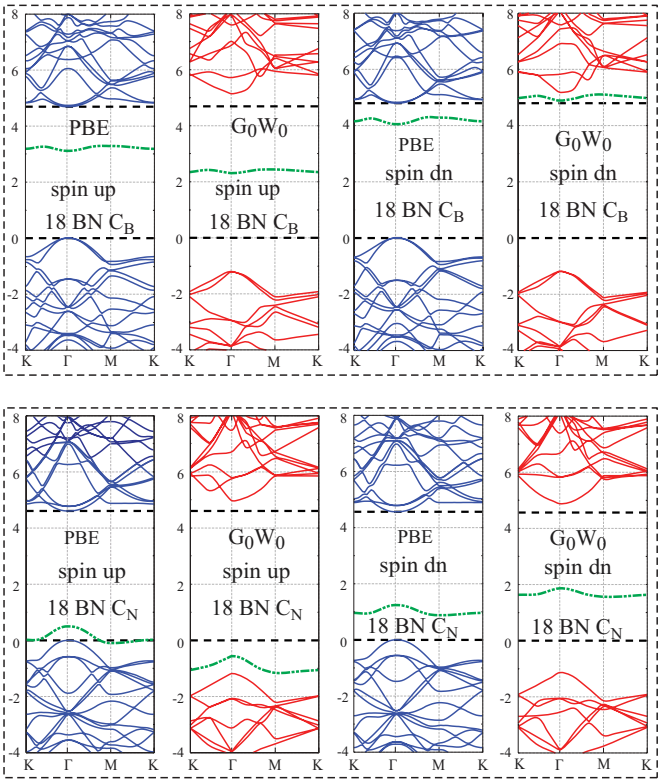

FIG. 8. (Color online) Electronic band structure of 18-atom BN supercell (at 10 Å vacuum separation) where a B or N atom is substituted with a C atom. Calculations are done involving PBE (blue lines) and G_0W_0 (red lines) approaches. Green dotted lines emphasize the impurity levels. Spin-up and spin-down results are presented. The top of the valence band within the PBE is taken as zero energy. The edges of the PBE band gap are indicated by black dashed horizontal lines. The Greek letters stand for high-symmetry points in the BZ of the supercell.

point. Taking into account the drop in E_f corresponding to B substitution at positive charge states,[31] C atoms may still predominately take the positions of B atoms even in the B-rich environment.

We also looked at the substitution process from a different perspective. Assuming that carbon adatoms appear on the h-BN sheet due to electron-beam-mediated dissociation of

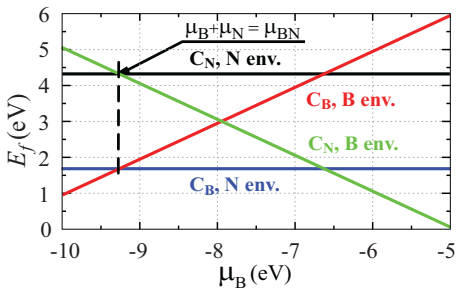

FIG. 9. (Color online) Energy required to substitute B and N atoms with C for the neutral charge states as functions of μ_B. The horizontal lines stand for the E_f of C_B and C_N configurations calculated in the N-rich environment. The vertical dotted line corresponds to the condition defined by Eq. (3).

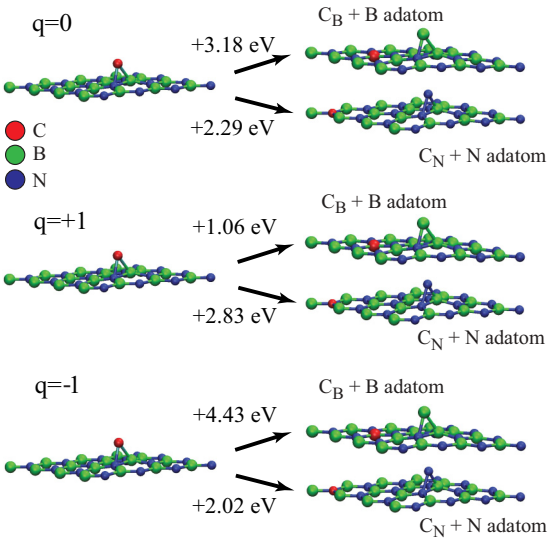

FIG. 10. (Color online) Difference in the total energy of the system for the neutral and charged states of the h-BN sheet with defects. C adatom on pristine h-BN sheet (reference system); C atoms in substitutional positions and the corresponding B or N adatom on the h-BN sheet are investigated. Numbers stand for the total-energy difference between the reference system and a configuration shown on the right side from the arrow. q stands for the charge. It is evident that positive charge decreases the formation energy of substitutional C impurity in the position of the B atom.

hydrocarbon molecules, we explored several neutral and charged systems with adatoms: with C adatom on the pristine BN sheet, and with C atoms in substitutional positions and the corresponding B or N adatom on the h-BN sheet (Fig. 10). The total-energy analysis of those systems (Fig. 10) demonstrates the same trend that was observed earlier in our work[31]—positive charging reduces the energy required to exchange a B atom with a C atom and makes it lower than the energy required to exchange an N atom with a C atom, while negative charge leads to the opposite situation. The lower formation energies of defects with N-terminating edges are consistent with the preferential substitution of B atoms reported in the experiments.[28,29]

D. Displacement energies and rates

The complete understanding of the substitution process under the electron beam is not possible without the microscopic knowledge of the dynamical effects. To estimate the role of kinetics in the process of carbon substitution, molecular dynamics simulations of electron impacts onto the h-BN monolayer were carried out. Since we are interested in the growth of carbon islands under electron-beam irradiation, displacement thresholds of C substitutional impurity (in the B- and N-atom position) as well as its nearest-neighbor B and N atoms were calculated. The displacement threshold (T_d) is the minimum kinetic energy that should be delivered to the atom to remove it from its position without immediate recombination. The corresponding electron threshold energy can be estimated[32,63] when T_d is known. In addition, when the displacement threshold is known, the estimation of the displacement rate (σ) can be done using the McKinley-Feshbach

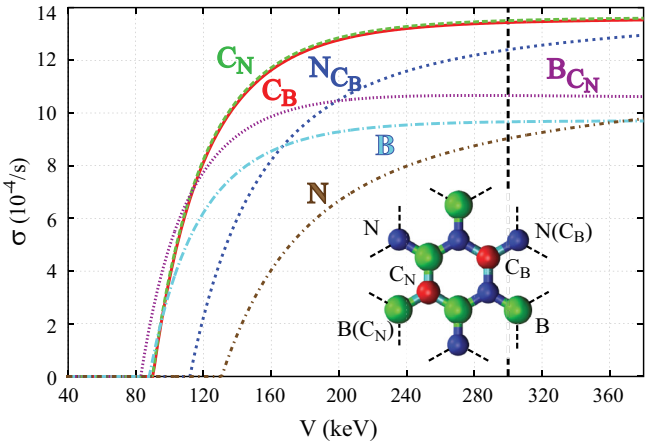

FIG. 11. (Color online) Displacement rates for B and N atoms in pristine systems, C atom in B and N position, nearest to the single C substitutional defect B and N atoms as functions of acceleration voltage (electron-beam energy). Black vertical dashed line indicates the value of the electron-beam energy used in the experiments (300 keV). All values were calculated at electron-beam current of 10.0 A/cm^2.

formalism for Coulomb scattering of relativistic electrons.[64] In the simulations, the h-BN sheet is oriented perpendicularly to the incident electron direction and thus maximum energy transfer from the incident electron to the atom is considered. Kinetic energy was instantaneously assigned to the recoil atom, and DFT molecular dynamics was used to investigate if the amount of energy was sufficient to take the atom away from the system. We neglected the effects of temperature[65,66] on the displacement thresholds, as they give rise to a tail just below the threshold only and do not change the shapes of the curves at higher voltages.

We found that T_d for the C atom (independent of the B or N atom substitution) is 1.5 eV less than for a B atom in the pristine system, giving a rise to a 30% increase in the displacement rate (for 300 keV used in the simulations) as compared to that for a B atom in the pristine material (Fig. 11). This means that the substitution of individual atoms can hardly be explained by dynamical effects only. The displacement threshold for the nearest B-neighbor atoms (C_N defect) drops by 1.2 eV, and by 3.6 eV for neighboring N atoms (C_B defect) as compared to the corresponding values in the pristine system. The knowledge of the displacement rates for different types of atoms, along with the information on the energetics of different configurations and partial pressure of the volatile components in the chamber, should make it possible to use the Monte Carlo methods to model the kinetics of the process.

IV. CONCLUSIONS

To conclude, using DFT approaches with local and non-local XC functionals and the GW method, we calculated the electronic structure of h-BN sheets. We considered both pristine systems and those doped with carbon. We showed that the fundamental band gap in 2D h-BN is different from the gap in the bulk material. We also demonstrated that due to the non-local nature of the GW approximation, the gap calculated using the GW approach depends on the interlayer separation between the images of the layers within the periodic supercell approach, so that the results corresponding to the isolated 2D system must be extrapolated to the limit of infinitely large separations between the images. We further showed by the example of carbon substitutional impurities that the local and hybrid XC functionals give a qualitatively correct picture of the impurity states in the gap. Finally, we address the effects of many important parameters such as the choice of chemical potential, and estimated atom displacement cross sections for the substitutional process during the electron-beam-mediated doping of h-BN sheets with carbon atoms. Our results shed light on the electronic structure of pristine and doped h-BN and should further help to optimize the postsynthesis doping of boron nitride nanostructures stimulated by the electron irradiation. Specifically, by using a focused electron beam and simultaneously charging the sample, one can manufacture spatially localized hybrid structures which should exhibit intriguing electronic and magnetic properties.[67,68] The technique, which can be referred to as a combination of electron irradiation and beam-assisted deposition, can be applied to various 2D materials, including recently reported non-organic 2D structures.[4] Indeed, filling of vacancies created by the electron beam in molybdenum disulfide was recently demonstrated in the experiments.[69]

ACKNOWLEDGMENTS

This work was supported by the Finnish Academy of Science and Letters, and the Academy of Finland through the Centre of Excellence and other projects. We also acknowledge the Finnish IT Center for Science (CSC) for generous grants of computer time.

[1]K. S. Novoselov, A. K. Geim, S. V. Morozov, D. Jiang, Y. Zhang, S. V. Dubonos, I. V. Grigorieva, and A. A. Firsov, Science **306**, 666 (2004).

[2]A. K. Geim and K. S. Novoselov, Nature Mater. **6**, 183 (2007).

[3]K. S. Novoselov, D. Jiang, F. Schedin, T. J. Booth, V. V. Khotkevich, S. V. Morozov, and A. K. Geim, PNAS **102**, 10451 (2005).

[4]J. N. Coleman, M. Lotya, A. O. Neill, S. D. Bergin, P. J. King, U. Khan, K. Young, A. Gaucher, S. De, R. J. Smith, I. V. Shvets, S. K. Arora, G. Stanton, H.-y. Kim, K. Lee, G. T. Kim, G. S. Duesberg, T. Hallam, J. J. Boland, J. J. Wang, J. F. Donegan, J. C. Grunlan, G. Moriarty, A. Shmeliov, R. J. Nicholls, J. M. Perkins, E. M. Grieveson, K. Theuwissen, D. W. Mccomb, P. D. Nellist, and V. Nicolosi, Science **331**, 568 (2011).

[5]B. Radisavljevic, a. Radenovic, J. Brivio, V. Giacometti, and a. Kis, Nature Nanotech. **6**, 147 (2011).

[6]D. Pacilé, J. C. Meyer, Ç. Ö. Girit, and A. Zettl, Appl. Phys. Lett. **92**, 133107 (2008).

[7]N. Alem, R. Erni, C. Kisielowski, M. D. Rossell, W. Gannett, and A. Zettl, Phys. Rev. B **80**, 155425 (2009).
[8]R. V. Gorbachev, I. Riaz, R. R. Nair, R. Jalil, L. Britnell, B. D. Belle, E. W. Hill, K. S. Novoselov, K. Watanabe, T. Taniguchi, A. K. Geim, and P. Blake, Small **7**, 465 (2011).
[9]J. C. Meyer, A. Chuvilin, G. Algara-Siller, J. Biskupek, and U. Kaiser, Nano Lett. **9**, 2683 (2009).
[10]D. Golberg, Y. Bando, Y. Huang, T. Terao, M. Mitome, C. Tang, and C. Zhi, ACS Nano **4**, 2979 (2010).
[11]X. Li, W. Cai, J. An, S. Kim, J. Nah, D. Yang, R. Piner, A. Velamakanni, I. Jung, E. Tutuc, S. K. Banerjee, L. Colombo, and R. S. Ruoff, Science **324**, 1312 (2009).
[12]S. Bae, H. Kim, Y. Lee, X. Xu, J. Park, Y. Zheng, J. Balakrishnan, T. Lei, H. R. Kim, Y. I. Song, Y.-J. Kim, K. S. Kim, B. Özyilmaz, J.-H. Ahn, B. H. Hong, and S. Iijima, Nature Nanotech. **5**, 574 (2010).
[13]K. S. Kim, Y. Zhao, H. Jang, S. Y. Lee, J. M. Kim, K. S. Kim, J.-H. Ahn, P. Kim, J.-Y. Choi, and B. H. Hong, Nature (London) **457**, 706 (2009).
[14]Q. Yu, L. A. Jauregui, W. Wu, R. Colby, J. Tian, Z. Su, H. Cao, Z. Liu, D. Pandey, D. Wei, T. F. Chung, P. Peng, N. P. Guisinger, E. A. Stach, J. Bao, S.-S. Pei, and Y. P. Chen, Nature Mater. **10**, 443 (2011).
[15]L. Song, L. Ci, H. Lu, P. B. Sorokin, C. Jin, J. Ni, A. G. Kvashnin, D. G. Kvashnin, J. Lou, B. I. Yakobson, and P. M. Ajayan, Nano Lett. **10**, 3209 (2010).
[16]K. Kim, A. Hsu, X. Jia, S. Kim, Y. Shi, M. Hofmann, D. Nezich, J. Rodriguez-Nieva, M. Dresselhaus, T. Palacios *et al.*, Nano Lett. **12**, 161 (2012).
[17]L. Ci, L. Song, C. H. Jin, D. Jariwala, D. X. Wu, Y. J. Li, A. Srivastava, Z. F. Wang, K. Storr, L. Balicas, F. Liu, and P. M. Ajayan, Nature Mater. **9**, 430 (2010).
[18]D. Wei, Y. Liu, Y. Wang, H. Zhang, L. Huang, and G. Yu, Nano Lett. **9**, 1752 (2009).
[19]A. L. M. Reddy, A. Srivastava, S. R. Gowda, H. Gullapalli, M. Dubey, and P. M. Ajayan, ACS Nano **4**, 6337 (2010).
[20]M. Kawaguchi, T. Kawashima, and T. Nakajima, Chem. Mater. **8**, 1197 (1996).
[21]K. Yuge, Phys. Rev. B **79**, 144109 (2009).
[22]J. da Rocha Martins and H. Chacham, ACS Nano **5**, 385 (2011).
[23]S. Cahangirov and S. Ciraci, Phys. Rev. B **83**, 165448 (2011).
[24]Y. Liu, S. Bhowmick, and B. I. Yakobson, Nano Lett. **11**, 3113 (2011).
[25]M. Qiu and K. M. Liew, J. Appl. Phys. **110**, 064319 (2011).
[26]A. Ramasubramaniam and D. Naveh, Phys. Rev. B **84**, 075405 (2011).
[27]Y. Xu, Z. Guo, H. Chen, Y. Yuan, J. Lou, X. Lin, H. Gao, H. Chen, and B. Yu, Appl. Phys. Lett. **99**, 133109 (2011).
[28]X. Wei, M. Wang, Y. Bando, and D. Golberg, J. Am. Chem. Soc. **132**, 13592 (2010).
[29]X. Wei, M. Wang, Y. Bando, and D. Golberg, ACS Nano **5**, 29162922 (2011).
[30]O. L. Krivanek, M. F. Chisholm, V. Nicolosi, T. J. Pennycook, G. J. Corbin, N. Dellby, M. F. Murfitt, C. S. Own, Z. S. Szilagyi, M. P. Oxley, S. T. Pantelides, and S. J. Pennycook, Nature (London) **464**, 571 (2010).
[31]N. Berseneva, A. V. Krasheninnikov, and R. M. Nieminen, Phys. Rev. Lett. **107**, 035501 (2011).
[32]J. Kotakoski, C. H. Jin, O. Lehtinen, K. Suenaga, and A. V. Krasheninnikov, Phys. Rev. B **82**, 113404 (2010).
[33]B. Huang and S.-H. Wei, Phys. Rev. Lett. **107**, 239601 (2011).
[34]N. Berseneva, A. V. Krasheninnikov, and R. M. Nieminen, Phys. Rev. Lett. **107**, 239602 (2011).
[35]G. Kresse and J. Furthmüller, Comput. Mater. Sci. **6**, 15 (1996).
[36]J. P. Perdew, K. Burke, and M. Ernzerhof, Phys. Rev. Lett. **77**, 3865 (1996).
[37]J. Heyd, G. E. Scuseria, and M. Ernzerhof, J. Chem. Phys. **118**, 8207 (2003).
[38]M. Shishkin, M. Marsman, and G. Kresse, Phys. Rev. Lett. **99**, 246403 (2007).
[39]M. Shishkin and G. Kresse, Phys. Rev. B **75**, 235102 (2007).
[40]O. Cretu, A. V. Krasheninnikov, J. A. Rodríguez-Manzo, L. Sun, R. M. Nieminen, and F. Banhart, Phys. Rev. Lett. **105**, 196102 (2010).
[41]A. V. Krasheninnikov, P. O. Lehtinen, A. S. Foster, P. Pyykkö, and R. M. Nieminen, Phys. Rev. Lett. **102**, 126807 (2009).
[42]J. Kotakoski, D. Santos-Cottin, and A. V. Krasheninnikov, ACS Nano **6**, 671 (2011).
[43]G. Cappellini, G. Satta, M. Palummo, and G. Onida, Phys. Rev. B **64**, 035104 (2001).
[44]B. Arnaud, S. Lebègue, P. Rabiller, and M. Alouani, Phys. Rev. Lett. **96**, 026402 (2006).
[45]X. Blase, A. Rubio, S. G. Louie, and M. L. Cohen, Phys. Rev. B **51**, 6868 (1995).
[46]L. Liu, Y. P. Feng, and Z. X. Shen, Phys. Rev. B **68**, 104102 (2003).
[47]H. Sahin, S. Cahangirov, M. Topsakal, E. Bekaroglu, E. Akturk, R. Senger, and S. Ciraci, Phys. Rev. B **80**, 155453 (2009).
[48]M. Topsakal, E. Aktürk, and S. Ciraci, Phys. Rev. B **79**, 115442 (2009).
[49]A. Nagashima, N. Tejima, Y. Gamou, T. Kawai, and C. Oshima, Phys. Rev. B **51**, 4606 (1995).
[50]K. Watanabe, T. Taniguchi, and H. Kanda, Nature Mater. **3**, 404 (2004).
[51]V. L. Solozhenko, A. G. Lazarenko, J.-P. Petitet, and A. V. Kanaev, J. Phys. Chem. Solids **62**, 1331 (2001).
[52]L. Wirtz, A. Marini, and A. Rubio, AIP Conf. Proc. **786**, 391 (2005).
[53]S. Wang, Q. Chen, and J. Wang, Appl. Phys. Lett. **99**, 063114 (2011).
[54]B. Arnaud, S. Lebègue, P. Rabiller, and M. Alouani, Phys. Rev. Lett. **96**, 026402 (2006).
[55]M. Shishkin, M. Marsman, and G. Kresse, Phys. Rev. Lett. **99**, 246403 (2007).
[56]B.-C. Shih, Y. Xue, P. Zhang, M. L. Cohen, and S. G. Louie, Phys. Rev. Lett. **105**, 146401 (2010).
[57]C. Friedrich, M. C. Müller, and S. Blügel, Phys. Rev. B **83**, 081101 (2011).
[58]M. Shishkin and G. Kresse, Phys. Rev. B **74**, 035101 (2006).
[59]A. Gulans (unpublished).
[60]J. C. Inkson, Surf. Sci. **28**, 69 (1971).
[61]J. P. A. Charlesworth, R. W. Godby, and R. J. Needs, Phys. Rev. Lett. **70**, 1685 (1993).
[62]M. H. Evans, J. D. Joannopoulos, and S. T. Pantelides, Phys. Rev. B **72**, 045434 (2005).
[63]A. Zobelli, A. Gloter, C. P. Ewels, G. Seifert, and C. Colliex, Phys. Rev. B **75**, 245402 (2007).

[64]W. A. McKinley and H. Feshbach, Phys. Rev. **74**, 1759 (1948).
[65]T. Susi, J. Kotakoski, R. Arenal, S. Kurasch, H. Jiang, V. Skakalova, O. Stephan, A. V. Krasheninnikov, E. I. Kauppinen, U. Kaiser, and J. C. Meyer, ACS Nano **6**, 8837 (2012).
[66]J. C. Meyer, F. Eder, S. Kurasch, V. Skakalova, J. Kotakoski, H. Park, S. Roth, A. Chuvilin, S. Eyhusen, G. Benner, A. V. Krasheninnikov, and U. Kaiser, Phys. Rev. Lett. **108**, 196102 (2012).
[67]J. Li and V. B. Shenoy, Appl. Phys. Lett. **98**, 013105 (2011).
[68]J. M. Pruneda, Phys. Rev. B **81**, 161409 (2010).
[69]H.-P. Komsa, J. Kotakoski, S. Kurasch, O. Lehtinen, U. Kaiser, and A. V. Krasheninnikov, Phys. Rev. Lett. **109**, 035503 (2012).